Chinese Chemical Letters 37 (2026) 111384

Contents lists available at ScienceDirect

Chinese Chemical Letters

journal homepage: www.elsevier.com/locate/cclet

Pyrazole-thermal-assisted assembly of the largest N-rich tin-oxo clusters with tunable broadband nonlinear optical limiting effect

Peng Li[a,1], Qian-Ru Sun[b,1], Chen-Bo Yu[c], Jia-Li Chen[b], Yu Zhu[a,b,*], Qian Zhou[a], Zi-Yan Guo[a], Shi-Yu Xiong[a], Jia-Heng Lv[a], Tian-Yun Fu[a], Chan Zheng[c,*], Qiao-Hong Li[b], Wei-Hui Fang[b], Jian Zhang[b], Dong-Sheng Li[a,*]

[a] Key Laboratory of Inorganic Nonmetallic Crystalline and Energy Conversion Materials, College of Materials and Chemical Engineering, China Three Gorges University, Yichang 443002, China
[b] State Key Laboratory of Structural Chemistry, Fujian Institute of Research on the Structure of Matter, Chinese Academy of Sciences, Fuzhou 350002, China
[c] Institute of Biology and Chemistry, Fujian University of Technology, Fuzhou 350118, China

ARTICLE INFO

Article history:
Received 8 March 2025
Revised 20 May 2025
Accepted 28 May 2025
Available online 28 May 2025

Keywords:
Tin-oxo cluster
Pyrazole-thermal synthesis
Organic-inorganic hybrid
Ligand regulation
Optical limiting

ABSTRACT

Tin-oxo clusters (TOCs) have attracted considerable attention owing to their various structures and wide potential applications. However, there is still a lack of effective methods to assemble high-nuclearity TOCs. Moreover, the periphery of reported TOCs is rarely N-rich ligands, limiting the comprehensive investigation of the structure-property relationship. In this work, we used the strategy of pyrazole-thermal-assisted organotin aggregation to construct a series of the largest N-rich Sn_{18} clusters with S_4 axial symmetry. These Sn_{18} clusters have inorganic electron-withdrawing halogen atoms and organic electron-rich pyrazole derivatives, differing from the reported high-nuclearity TOCs only with carboxylate ligands. Owing to the high symmetry and multiple electron-withdrawing/-donating ligands, the Sn_{18} clusters served as the platform to investigate the relationship between structure and third-order nonlinear optical (NLO) property by Z-scan measurement. Different from the single organic ligand in the previous study, the multiple kinds of ligands in the Sn_{18} clusters have an important effect on the NLO property. Enhancing the push-pull electronic effect and introducing C–Cl···π interactions between different ligands can promote the NLO properties. Thus, CTGU-SnC-16 exhibits the best broadband NLO properties at 532 and 1064 nm, differing from the reported metal-oxo clusters only at 532 nm. This work not only affords an effective synthetic strategy for constructing high-nuclearity TOCs but also deepens the understanding of the structure-property relationship of clusters.

© 2026 Published by Elsevier B.V. on behalf of Chinese Chemical Society and Institute of Materia Medica, Chinese Academy of Medical Sciences.

Tin-oxo clusters (TOCs), as the molecular model of tin oxide materials, have aroused increasing interest owing to their various potential applications in many fields, such as extreme ultraviolet lithography, electrocatalytic CO_2 reduction, catalysis, and nonlinear optics [1–6]. The crystalline TOCs can provide precise atomic structural information for deeply understanding the structure-property relationship at the molecular level [7–9]. Currently, many types of TOCs with organic ligands were reported [10–15], such as typical drum-like $\{R'SnO(O_2CR)\}_6$ [16], cubic $[n\text{-BuSn(O)}O_2P(t\text{-Bu})_2]_4$ [17], double *O*-capped $[\{(n\text{-BuSn})_3(PhO)_3O\}_2\{HPO_3\}_4]$ [18], wheel-like $[(n\text{-BuSn})_{18}O_{18}(H_2\text{-DBA})_{12}(DBA)_2]$ [19], rod-like $[(n\text{-BuSn})_{22}Sn_4(OH)_{26}O_{22}(IANO)_6]^{6+}$ [20], and dimeric $[(n\text{-BuSn})_{34}Na_2(OH)_{14}O_{40}(PA)_8]^{2+}$ [20]. These TOCs can combine the advantages of inorganic and organic composites with flexible and accurate variation, allowing the opportunity to modify and eventually optimize the properties. Despite the prominent progress in TOC chemistry, the diversity of TOCs remains less developed. Most reported TOCs have low nuclear cores, and the number above pentadeca-nuclearity is only ten [19–22]. Moreover, the peripheral ligands are mainly the O-containing ligands, such as carboxylate or phosphonate, and rarely the N-rich ligands [23–25]. These all limit the expansion of the application and comprehensive investigation of the structure-property relationship. The synthetic method, Sn source, and coordination tendency of the Sn atom are important factors influencing the structures of TOCs. In the previous synthesis, the steric hindrance of organotin brings difficulty in constructing high-nuclearity structures, while the inorganic

* Corresponding authors.
E-mail addresses: zhuyu@ctgu.edu.cn (Y. Zhu), czheng@fjut.edu.cn (C. Zheng), lidongsheng1@126.com (D.-S. Li).
[1] These authors contributed equally to this work.

https://doi.org/10.1016/j.cclet.2025.111384
1001-8417/© 2026 Published by Elsevier B.V. on behalf of Chinese Chemical Society and Institute of Materia Medica, Chinese Academy of Medical Sciences.

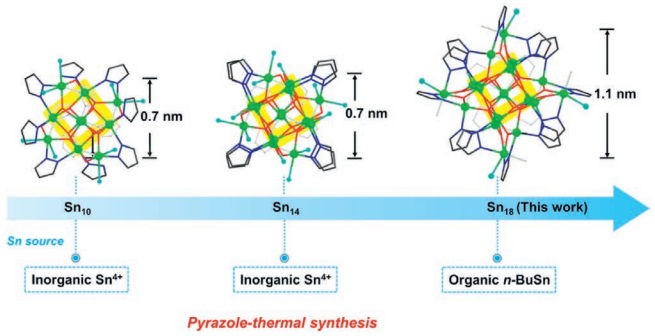


Fig. 1. Illustration of the structural expansion from the N-rich Sn_{10} to Sn_{18} cluster using different Sn sources by pyrazole-thermal synthesis. Terminal butyl groups of the Sn_{18} cluster were omitted for clarity. Atom color code: green Sn; bright blue Cl.

Sn ion is easily hydrolyzed to oxide precipitation [26]. The Sn atoms generally favor coordinating with oxygen atoms rather than nitrogen atoms. Therefore, it is challenging but attractive work to assemble the N-rich high-nuclearity TOCs.

In the past decades, many efforts have been made to explore the synthesis of high-nuclearity TOCs, including conventional solution synthesis and solvothermal synthesis [27–33]. The conventional solution synthesis is limited by the solubility of all the starting chemicals [34]. And nearly all the obtained TOCs with functional ligands are low-nuclear [26]. The solvothermal synthesis with high pressure and temperature can prompt the dissolution of the starting chemicals. It has successfully made several high-nuclearity TOCs with functional ligands using the organotin precursor, including our previous work about Sn_{26} clusters [20]. Most resulting high-nuclearity TOCs are close-packing organic-inorganic cores and need the inorganic Sn atoms as the linkers. These inorganic Sn atoms either depend on the *in situ* cleavage of the Sn-C bond in the butyltin or the additional introduction of inorganic Sn salt [20,22]. However, it is difficult to form inorganic Sn atoms through *in situ* cleavage of the Sn-C bond or control the hydrolysis of inorganic Sn salt in solvothermal synthesis. Therefore, it is urgent to explore a new approach to constructing targeted high-nuclearity TOCs.

Based on our previous work about high-nuclearity TOCs, we decided to adopt pyrazole as a reaction medium to assist the cleavage of Sn-C bonds of butyltin and assemble the N-rich high-nuclearity TOCs. According to the characteristics of organometallic bonds, the pyrazole with alkalinity can act as the nucleophilic reagent to attack organotin, resulting in the cleavage of Sn-C bonds. This guarantees sufficient inorganic Sn atoms for further assembly, which differs from the few production of inorganic Sn atoms in solvothermal synthesis. Moreover, the electron-rich pyrazole as the N-rich π-conjugated ligand can not only play the role of a bridge to construct TOCs but also endow the intriguing properties for the whole cluster [35].

Following this synthetic strategy, the N-rich high-nuclearity structure $[(n\text{-BuSn})_{12}Sn_6O_{20}(PZ)_{16}Cl_4]$ (HPZ = pyrazole, CTGU-SnC-11) was successfully synthesized. The Sn_{18} cluster in the CTGU-SnC-11 is the S4 axisymmetric structure with two types of ligands, inorganic electron-withdrawing Cl atoms and organic electron-rich pyrazole ligands. It is different from the reported high-nuclearity TOCs only with carboxylate ligands. The size of this Sn_{18} cluster core reaches up to 1.1 nm (Fig. 1), the largest N-rich tin-oxo cluster in the TOCs chemistry. The number of its nuclearity is higher than the reported N-rich Sn_{10} and Sn_{14} clusters obtained by the inorganic Sn salt in pyrazole-thermal synthesis, demonstrating the effectiveness of this synthetic strategy [24,25]. Considering the push-pull electronic effect between different ligands and intermolecular forces, we decided to modulate the ligands from two aspects for further investigating the structure-property relationship: (1) Expanded the synthetic method to other pyrazole derivatives with electron-donating -CH_3 group or Cl atom; (2) Introduced the stronger electron-withdrawing F anions to replace the Cl anions. Subsequently, a series of N-rich Sn_{18} clusters $[(n\text{-BuSn})_{12}Sn_6O_{20}(L)_{16\times4}]\cdot$Guest (X = Cl, Guest = $4H_2O$: HL = 4-methyl-pyrazole ($HPZCH_3$) (CTGU-SnC-12), 4–chloro–pyrazole (HPZCl) (CTGU-SnC-13); X = F: *L* = PZ, Guest = $2H_2O$ (CTGU-SnC-14); L = $PZCH_3$, Guest = $HPZCH_3\cdot5H_2O$ (CTGU-SnC-15); L = PZCl, Guest = $4H_2O$ (CTGU-SnC-16) were successfully assembled. The third-order nonlinear optical (NLO) properties of the Sn_{18} family were further investigated by Z-scan measurement. They exhibit excellent broadband NLO properties at 532 and 1064 nm, differing from the reported metal-oxo clusters only at 532 nm [36–39]. Furthermore, their NLO properties can be modulated by precise structural regulation.

Colorless crystals of CTGU-SnC-11 were prepared by the reaction of butyltin hydroxide oxide, pyrazole, NaCl, and 2-picolinic acid at 100 °C. The melting point of pyrazole is 66–70 °C. It is solid at room temperature and becomes liquid above the melting point. It acts as the solvent and participates in the assembly of TOCs. During the reaction process, the Sn-C bond of butyltin is cleaved to form the inorganic Sn atom with the assistance of pyrazole (Fig. 2a). One central inorganic Sn atom is linked to three butyltins and another inorganic Sn atom through five oxygen atoms, forming the $(n\text{-BuSn})_3Sn_2$ pentagram with a truncated corner. During the experiment, the reaction mixture after a two-day reaction was analyzed by electrospray ionization mass spectrometry (ESI-MS) using methanol as the spray solvent. As shown in Fig. S1 (Supporting information), prominent MS signals are observed at *m/z* 1352.9364 and 1398.9778, corresponding to $[(n\text{-BuSn})_3Sn_2O_6(PZ)_4(CH_3OH)_7]^+$ (simulated signal: 1352.9946) and $[(n\text{-BuSn})_3Sn_2O_5Cl_2(PZ)_4(CH_3OH)_5(H_2O)_3]^+$ (simulated signal: 1398.9154), respectively. The methanol molecules in these formulas are attributed to the spray solvent. These results confirm the formation of $(n\text{-BuSn})_3Sn_2$ units during the reaction, thereby demonstrating the auxiliary role of pyrazole in the synthesis. In the resulting Sn_{18} cluster, two $(n\text{-BuSn})_3Sn_2$ units are gathered by sharing one limbic inorganic Sn atom. Then two dimers are further connected by four pairs of oxygen atoms of the $(n\text{-BuSn})_3Sn_2$ units, forming an octadeca-nuclearity cluster. All the inorganic Sn atoms display octahedral geometry with two different coordination environments: SnO_5N and SnO_4N_2 octahedra. In the SnO_5N octahedron, the Sn atom is located in the center of the $(n\text{-BuSn})_3Sn_2$ unit and coordinated by four equatorial oxygen atoms of the $(n\text{-BuSn})_3Sn_2$ unit, one oxygen atom of the adjacent $(n\text{-BuSn})_3Sn_2$ unit, and one N atom of the pyrazole ligand. The SnO_4N_2 octahedron is defined by two oxygen atoms of a $(n\text{-BuSn})_3Sn_2$ unit, two oxygen atoms of another $(n\text{-BuSn})_3Sn_2$ unit, and two N atoms of two pyrazole ligands. The organic Sn atoms all surround the inorganic Sn centers and have a distorted SnO_4CN, SnO_2CN_2Cl, or SnO_2CN_3 octahedral environment. The pyrazole ligands all take on the bridging role through two N sites in the whole structure. These N-rich π-conjugated pyrazole ligands are situated in the periphery of the Sn_{18} core, forming the electron-rich shell.

Single-crystal X-ray diffraction analysis indicates that CTGU-SnC-11 crystallizes in the *I*-4 space group (Table S1 and Fig. S2 in Supporting information). By carefully analyzing the structure, the Sn_{18} cluster has the S4 axis of symmetry. It is worth noting that the Sn_{10} and Sn_{14} clusters obtained by pyrazole-thermal synthesis also have the S4 axis of symmetry (Fig. 2b). The increasing Sn atoms from the Sn_{10} to Sn_{18} cluster are arranged in the S4 axial symmetry. In the Sn_{10} cluster, the central $\{Sn_4\}$ unit is placed in the non-planar quadrangle. After adding four Sn atoms, the central moiety transforms into a distorted cube-like $\{Sn_8\}$ unit to form the Sn_{14} cluster. Based on the Sn_{14} structure, four pairs of

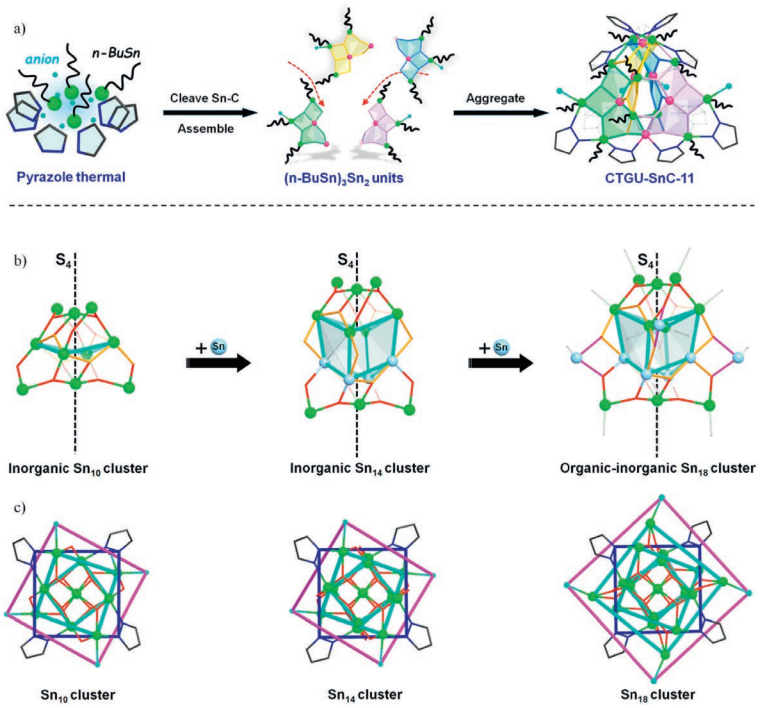


Fig. 2. (a) The assembly process of CTGU-SnC-11 through the strategy of pyrazole-thermal-assisted organotin aggregation. (b) The gradually increasing nuclearities from the inorganic Sn_{10} cluster, *via* the Sn_{14} cluster, to the organic-inorganic hybrid Sn_{18} cluster with S_4 axis of symmetry. (c) Topological drawings of Sn_{10}, Sn_{14}, and Sn_{18} clusters in the S_4 axial symmetry. Terminal butyl groups of the Sn_{18} cluster were omitted for clarity. Atom color code: green/light blue Sn; bright blue Cl.

peripheral μ_2-O atoms capture four additional Sn atoms to form the Sn_{18} core. Differing from the inorganic tin-oxo core in the Sn_{10} and Sn_{14} clusters, the peripheral Sn atoms of Sn_{18} are all bonded to butyl groups, forming the organic-inorganic hybrid tin-oxo core. As shown in Fig. 2c, their structural evolution can be simplified in the S4 axial symmetry. In the Sn_{10} cluster, two non-planar $\{Sn_4\}$ squares around the central two Sn atoms are decorated with two squares of pyrazole ligands and chlorine atoms. On this basis, one additional non-planar $\{Sn_4\}$ square is superimposed on the intimal $\{Sn_4\}$ square to form the simplified Sn_{14} structure. Therefore, the size of the Sn_{14} cluster core is the same as that of the Sn_{10}. Compared to the Sn_{10} and Sn_{14} structures, there is an additional $\{Sn_4\}$ square outside the square of pyrazole ligands, and the chlorine atoms become the outermost square in the Sn_{18} cluster. This indicates that pyrazole-thermal-assisted organotin aggregation is an effective method for assembling high-nuclearity TOCs.

The Sn_{18} cluster has two different ligands, electron-withdrawing inorganic Cl atoms and electron-donating π-conjugated pyrazole ligands. The push-pull electronic effect between these different ligands would have an important influence on the properties of the whole cluster, especially the NLO performance. Therefore, we would modulate the kinds of ligands from two aspects for further systemic study of the structure-property relationship (Fig. 3). On the one hand, we expanded the pyrazole-thermal-assisted organotin aggregation strategy to other pyrazole derivatives with low melting points, such as 4-methyl-pyrazole and 4–chloro–pyrazole. Thus, the electron-donating methyl group and chlorine atom were introduced to the pyrazole ring. Two Sn_{18} clusters with $PZCH_3$ and PZCl ligands, namely CTGU-SnC-12 and CTGU-SnC-13, were successfully constructed (Figs. S3 and S4 in Supporting information). On the other hand, the inorganic chlorine atoms were adjusted to the stronger electron-withdrawing fluorine atoms. Consequently, a series of F-decorating Sn_{18} clusters with different pyrazole derivatives were made, designated CTGU-SnC-14, CTGU-SnC-15, and CTGU-SnC-16 (Figs. S5-S7 in Supporting information).

The crystal structures of CTGU-SnC-12 to CTGU-SnC-16 were determined by single-crystal X-ray diffraction (Tables S1 and S2 in Supporting information). The structures of CTGU-SnC-12 to CTGU-SnC-16 are similar to that of CTGU-SnC-11 with an S4 axis of symmetry. Four Cl sites and sixteen PZ ligands of the original Sn_{18} cluster are all replaced by four F atoms and sixteen $PZCH_3$/PZCl ligands, respectively. The coordination modes of $PZCH_3$/PZCl ligands are the same as those of the PZ ligand, which bridges two Sn atoms *via* two N sites (Fig. S14 in Supporting information). In these clusters, each core contains a central inorganic Sn_6 moiety encapsulated by $(n\text{-BuSn})_{12}$ moiety (Fig. S15 in Supporting information). This Sn_{18} family can serve as a good platform to investigate the effect of multiple functional ligands on the NLO absorption and OL behaviors, which is different from the reported work about single π-conjugated ligands in the field of metal-oxo clusters. Furthermore, the Sn_{18} family was carefully characterized using powder X-ray diffraction (PXRD), infrared spectroscopy (IR), thermogravimetric analysis (TGA), and UV–vis spectroscopy (Figs. S21-S44 in Supporting information). As shown in Figs. S21-S26, the experimental PXRD patterns of these compounds can match well with the simulated patterns, indicating the phase purity of the crystal samples. In the IR spectra, the absorption bands at 3290–3313 cm^{-1} are assigned to the -OH stretching vibrations of solvent water molecules. The vibrations observed at 2962–2974, 2923–2929, and 2856–2884 cm^{-1} correspond to the C–H of heterocycle, the C–H and -CH_2- of the butyl groups, respectively. The vibrations at 1365–1388 and 1262–1279 cm^{-1} are assigned to the C–N of heterocycles and C–C of the butyl groups. The absorption peaks at 674–688 cm^{-1} are attributed to ν(O-Sn-O).

The high symmetry of the cluster structures and multiple electron-withdrawing/-donating ligands contributed to the NLO properties. Therefore, the NLO absorption and OL behaviors of the samples were explored in the picosecond regimes by the well-established OA Z-scan technology at 532 and 1064 nm. Figs. 4a and b depict the OA Z-scan plots of the samples at 532 and 1064 nm,

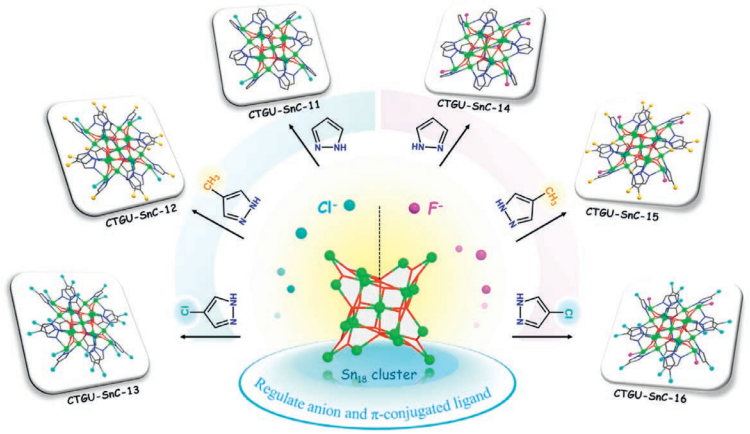


Fig. 3. The regulation of inorganic anions and organic pyrazole derivatives ligands in the Sn_{18} family. Terminal butyl groups of the Sn_{18} clusters were omitted for clarity. Atom color code: green Sn; bright blue Cl; purple red F; yellow C.

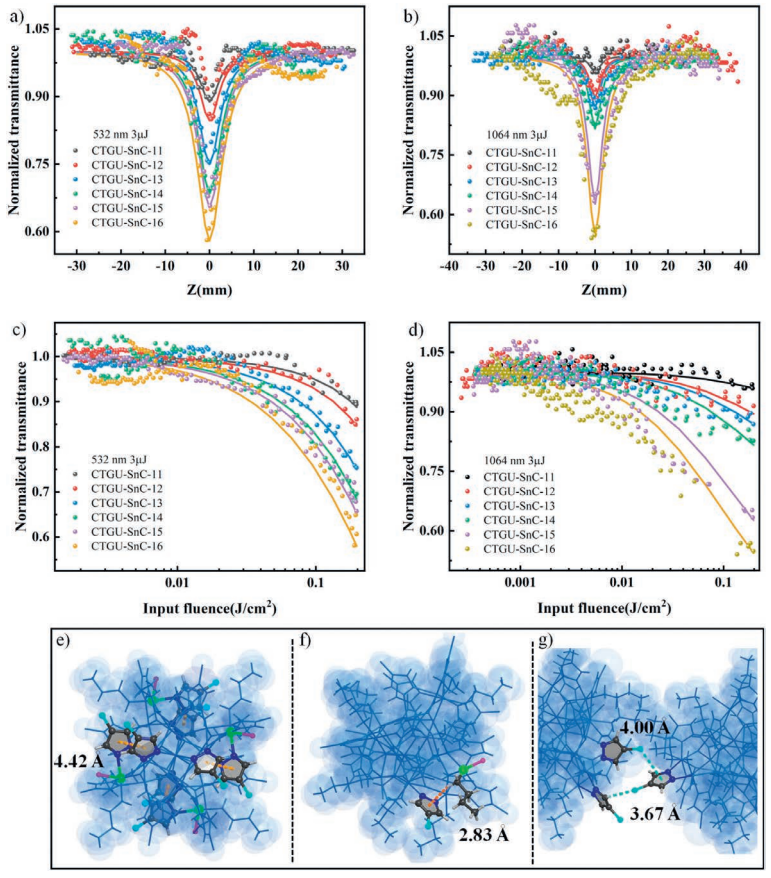


Fig. 4. (a, b) OA Z-scan curves and (c, d) OL curves of the samples at picosecond laser duration excitation with a wavelength of 532 and 1064 nm, respectively (input energy: 3 μJ). Scattered squares indicate experimental data with the solid line representing the curve of best fit. (e) $\pi\cdots\pi$ interactions between adjacent pyrazole rings, (f) C–H$\cdots\pi$ interactions between pyrazole ring and H atom of butyl group, (g) C–Cl$\cdots\pi$ interactions between Cl atom of PZCl ligand and adjacent pyrazole ring in CTGU-SnC-16.

respectively. From Figs. 4a and b, it is evident that the transmittance progressively decreased with enhancing the incident intensity of the excitation laser. All the Z-scan traces presented negative valleys at both 532 and 1064 nm wavelength, with minimum transmittance at the laser beam's focal point, indicating the typical reverse saturable absorption (RSA), which is attributed to the absorption of multiple photons when samples are irradiated using a high-fluence laser beam. At an excitation wavelength of 523 nm (*i.e.*, a photon energy of ~2.33 eV), the RSA is primarily derived from two-photon absorption (2PA) because for all investigated samples, $h\nu < E_g < 2h\nu$. However, at 1064 nm (*i.e.*, a photon energy of ~1.16 eV), $3h\nu < E_g < 4h\nu$, therefore, four-photon absorption (4PA) is responsible for the RSA. The measured Z-scan data can be fitted by a typical nonlinear absorption theory. The normalized transmission (T) was calculated as follows [1]:

$$T = \sum_{m=0}^{\infty} \frac{-\beta I_0 L_{\text{eff}} / \left(1 + \frac{z^2}{z_0^2}\right)}{(m+1)^{3/2}} \quad (1)$$

where I_0 is the peak intensity at the laser beam's focal point, β is the NLA coefficient, L_{eff} is the effective thickness, and z_0 is the Rayleigh. The fitting results are given as solid lines in Figs. 4a and b. The imaginary third-order optical susceptibility ($\text{Im}\chi^{(3)}$), which is determined by β, can be given by [2]:

$$\text{Im}\chi^{(3)} = \left(\frac{10^{-7} c\lambda n_0^2}{96\pi^2}\right) \cdot \beta \quad (2)$$

where c is the speed of light, λ is the laser wavelength, and n_0 is the linear refractive index of the tested sample.

The calculated NLO parameters are displayed in Table S15 (Supporting information). The value of β, $\text{Im}\chi^{(3)}$, and the figure of merit (FOM) of the samples showed similar trends at 532 and 1064 nm. Their values are increased in the following order: CTGU-SnC-11 < CTGU-SnC-12 < CTGU-SnC-13 < CTGU-SnC-14 < CTGU-SnC-15 < CTGU-SnC-16. This trend is not only related to the push-pull electronic effect between inorganic halogen atoms and organic electron-donor systems but also associated with C–Cl···π interactions between adjacent clusters. Firstly, the NLO properties of the F-decorating Sn_{18} clusters are all better than those of the Cl-decorating Sn_{18} clusters owing to the stronger push-pull electronic effect between the F atom and the electron-donor system. As shown in Fig. 4e and Figs. S16a-S20a (Supporting information), there are $\pi\cdots\pi$ interactions (4.34–4.91 Å) between the four pairs of adjacent electron-rich pyrazole rings. Besides this, the C–H···π interactions (2.72–2.83 Å) exist between the pyrazole rings and the H atoms of the butyl groups (Fig. 4f and Figs. S16b-S20b in Supporting information). These electron-donor systems are connected to the electron-withdrawing halogen atoms through one Sn atom. Therefore, the stronger electron-withdrawing abilities of halogen atoms generate a more significant push-pull electronic effect, leading to enhanced NLO properties for the Sn_{18} clusters. Furthermore, to verify this point, the electronic structures of typical Sn_{18} clusters with different halogen atoms, CTGU-SnC-13 (Cl), CTGU-SnC-14 (F) and CTGU-SnC-16 (F), were investigated through theoretical calculations. As shown in Fig. S45 (Supporting information), the lowest unoccupied molecular orbitals (LUMOs) of these clusters are essentially identical and primarily delocalized over the cluster cores. However, the highest occupied molecular orbitals (HOMOs) of the CTGU-SnC-13, CTGU-SnC-14 and CTGU-SnC-16 exhibit significantly different electron cloud distributions. The HOMO of CTGU-SnC-13 is delocalized across both the cluster core and the ligands. In contrast, the HOMO of CTGU-SnC-14 exhibits a higher electron density on the ligands and a lower density on the cluster core. The CTGU-SnC-16 shows predominant delocalization of the HOMO across the ligands. This results in stronger HOMO-to-LUMO electron transfer in CTGU-SnC-14 and CTGU-SnC-16 compared to compound CTGU-SnC-13, thereby improving the NLO properties. It is consistent with the experimental result, which demonstrates the critical role of the strong electron-withdrawing F atom. Secondly, the Cl atoms of the PZCl ligands in the Sn_{18} cluster have the C–Cl···π interactions (3.67–4.08 Å) with the pyrazole ring of the adjacent cluster (Fig. 4g and Fig. S18c in Supporting information). This is beneficial for electron transmission, which can promote nonlinear absorption. Thus, when the inorganic halogen atoms are the same in the structures, the NLO properties of the Sn_{18} clusters with PZCl ligands are better than those with PZ/$PZCH_3$ ligands. In addition, the introduction of electron-donating group can enhance the NLO properties [39]. Therefore, owing to the electron-donating -CH_3 group, the NLO properties of the Sn_{18} clusters with $PZCH_3$ ligands are better than those of Sn_{18} clusters with PZ ligands. All in all, the nonlinear absorption coefficient of the samples can be facilely controlled by regulation of cluster structure and multiple ligands.

The strong RSA response of the samples demonstrated that they show potential for use in OL. Therefore, the OL effects of the samples were manifested by plotting the normalized transmittance versus the input energy density, as calculated from the corresponding OA Z-scan measurements in Figs. 4a and b, as shown in Figs. 4c and d, respectively. The position-dependent light fluence $F_{\text{in}}(z)$ at any position z can be calculated from the corresponding beam radius $\omega(z)$ and the input laser pulse energy E_{in} through the following equation [3]:

$$F_{\text{in}}(z) = 4\sqrt{\ln 2}\left(\frac{E_{in}}{\pi^{3/2}}\right)(\omega(z))^2 \quad (3)$$

where $\omega(z)$ is provided by [4]:

$$\omega(z) = \omega(0)\sqrt{1 + (z/z_0)^2} \quad (4)$$

It can be seen from Figs. 4c and d that all samples showed identical behavior, wherein T remained constant at low input fluence and then continuously decreased with increasing fluence, clearly illustrating the presence of an OL effect. From the related OL parameters exhibited in Table S15, it is evident that the OL performance of the samples can also be adjusted by structural control. In addition, all the samples show excellent OL properties at 532 and 1064 nm. To date, almost all reported metal-oxo clusters have exhibited OL effects at 532 nm under nanosecond laser irradiation, while only a few Al-oxo clusters have demonstrated responses to picosecond lasers [36–42]. However, no studies have documented such effects in the infrared spectral region. In contrast, the Sn_{18} clusters not only exhibit excellent tunable broadband OL performance for picosecond laser pulses but also maintain stable normalized transmittance across multiple wavelengths, particularly in the case of CTGU-SnC-16. Furthermore, the OL performance of CTGU-SnC-16 surpasses that of the reported Al-oxo clusters under picosecond laser irradiation [36]. In addition, although some carbon-based composites exhibit responses to 532 nm (nanosecond) and 800/1030 nm (femtosecond) lasers, their normalized transmittance sharply decreases when the wavelength shifts from 532 nm to 800/1030 nm [43,44]. These imply that the Sn_{18} clusters can be applied as broadband optical limiters to protect human eyes and optical devices from inevitable damage induced by high-power lasers and exhibit great potential applications in optoelectronic fields.

In summary, we have developed a new strategy of pyrazole-thermal-assisted organotin aggregation to assemble a series of the largest N-rich tin-oxo clusters. The pyrazole derivatives not only assist the formation of sufficient inorganic Sn nodes through the cleavage of Sn-C bonds but also take the bridging role for constructing high-nuclearity TOCs. Differing from the reported high-nuclearity TOCs only with carboxylate ligands, the resulting Sn18 clusters with S4 axisymmetry are functionalized with multiple types of ligands, including inorganic electron-withdrawing halogen atoms and organic electron-rich pyrazole derivatives. These are conducive to the NLO properties of the Sn_{18} clusters, especially their push-pull electronic effect and C–Cl···π interactions. With the enhancement of the push-pull electronic effect, the NLO properties of the Sn_{18} family are increasing. And they exhibit excellent NLO properties at 532 and 1064 nm and promise to be broadband optical limiters. It is distinguished from the reported metal-oxo clusters only at 532 nm. This work not only offers an effective way to assemble high-nuclearity TOCs but also gives insight into modulating the broadband OL performance of metal-oxo clusters.

CRediT authorship contribution statement

Peng Li: Writing – original draft, Investigation. **Qian-Ru Sun:** Writing – original draft, Investigation. **Chen-Bo Yu:** Investigation. **Jia-Li Chen:** Data curation. **Yu Zhu:** Writing – review & editing, Supervision, Conceptualization. **Qian Zhou:** Investigation. **Zi-Yan Guo:**

Investigation. **Shi-Yu Xiong:** Investigation. **Jia-Heng Lv:** Investigation. **Tian-Yun Fu:** Investigation. **Chan Zheng:** Writing – review & editing, Supervision. **Qiao-Hong Li:** Supervision. **Wei-Hui Fang:** Supervision. **Jian Zhang:** Supervision. **Dong-Sheng Li:** Writing – review & editing, Supervision.

Declaration of competing interest

The authors declare that they have no known competing financial interests or personal relationships that could have appeared to influence the work reported in this paper.

Acknowledgments

This work is supported by the National Natural Science Foundation of China (Nos. 22371165, 22371278, 22001146, and U23A2095), the Scientific Research Project of the Education Department of Hubei Province (No. Q20211201), and the 111 Project (No. D20015).

Supplementary materials

Supplementary material associated with this article can be found, in the online version, at doi:10.1016/j.cclet.2025.111384.

References

[1] B. Cardineau, R.D. Re, M. Marnell, et al., Microelectron. Eng. 127 (2014) 44–50.
[2] M.C. Sharps, D.A. Marsh, L.N. Zakharov, et al., Res. Technol. 52 (2017) 521700081.
[3] A. Yanangisawa, H. Inoue, M. Morodome, et al., J. Am. Chem. Soc. 115 (1993) 10356–10357.
[4] A. Orita, A. Mitsutome, J. Otere, J. Org. Chem. 63 (1998) 2420–2421.
[5] Y. Zhu, D.S. Li, J. Zhang, et al., Chem. Comm. 58 (2022) 5650–5652.
[6] Y. Zhu, Z.R. Wang, D.J. Li, et al., Angew. Chem. Int. Ed. 61 (2022) e202202853.
[7] Y.B. Dong, H.Y. Shi, J. Yang, et al., Cryst. Growth Des. 15 (2015) 1546–1551.
[8] M. Hanif, M. Hussain, S. Ali, et al., Polyhedron 29 (2010) 613–619.
[9] A.S. Sougoule, Z. Mei, X. Xiao, et al., J. Organomet. Chem. 758 (2014) 19–24.
[10] V. Chandrasekhar, K. Gopal, S. Nagendran, et al., Cryst. Growth Des. 6 (2022) 267–273.
[11] B. Zobel, J. Costin, B.R. Vincent, et al., J. Chem. Soc., Dalton Trans. (2000) 4021–4022.
[12] Y. Zhu, M.R. Olsen, M. Nyman, et al., Inorg. Chem. 58 (2019) 4534–4539.
[13] R.O. Day, J.M. Holmes, V. Chandrasekhar, et al., J. Am. Chem. Soc. 109 (1987) 940–941.
[14] V. Chandrasekhar, P. Thilagar, J.F. Bickley, et al., J. Am. Chem. Soc. 127 (2005) 11556–11557.
[15] Q.F. Wang, C.L. Ma, G.F. He, et al., Polyhedron 49 (2013) 177–182.
[16] V. Chandrasekhar, R.O. Day, R.R. Holmes, Inorg. Chem. 24 (1985) 1970–1971.
[17] R.R. Holmes, K.C.K. Swamy, C.G. Schmid, et al., J. Am. Chem. Soc. 110 (1988) 7060–7066.
[18] V. Chandrasekhar, V. Baskar, J.J. Vittal, J. Am. Chem. Soc. 125 (2003) 2392–2393.
[19] Y. Zhu, Q.H. Li, D.S. Li, et al., Chem. Commun. 57 (2021) 5159–5162.
[20] Y. Zhu, L. Zhang, J. Zhang, Chem. Sci. 10 (2019) 9125–9129.
[21] J. Ayari, C.R. Göb, I.M. Oppel, Angew. Chem. Int. Ed. 59 (2020) 23892–23898.
[22] X.J. Tian, Y.Z. Yu, Q. Lu, Inorg. Chem. 61 (2022) 6037–6044.
[23] R.R. Holmes, Acc. Chem. Res. 22 (1989) 190–197.
[24] D. Wang, Z.N. Chen, Q.R. Ding, et al., CCS Chem. 2 (2020) 2607–2616.
[25] D. Wang, X.F. Yi, L. Zhang, Sci. China Chem. 65 (2022) 114–119.
[26] V. Chandrasekhar, K. Gopal, P. Thilagar, Acc. Chem. Res. 40 (2007) 420–434.
[27] G. Prabusankar, B. Jousseaume, T. Toupance, et al., Angew. Chem. Int. Ed. 45 (2006) 1255–1258.
[28] X. Xiao, K.Z. Shao, L.S. Yan, et al., Dalton Trans. 42 (2013) 15387–15390.
[29] F. Ribot, E. Martinez-Ferrero, K. Boubekeur, et al., Inorg. Chem. 47 (2008) 5831–5840.
[30] H. Reuter, Angew. Chem. Int. Ed. 30 (1991) 1482–1484.
[31] Y. Zhu, J. Zhang, L. Zhang, Inorg. Chem. 58 (2019) 15692–15695.
[32] G.L. Zheng, J.F. Ma, Z.M. Su, et al., Angew. Chem. Int. Ed. 43 (2004) 2409–2411.
[33] C.L. Ma, Y. Ren, Y.R. Wang, et al., Polyhedron 29 (2010) 881–885.
[34] L.M. Cui, W.H. Fang, J. Zhang, Chin. Chem. Lett. 36 (2025) 110386.
[35] Z.R. Wang, S.H. Shen, Y.P. Han, et al., Chin. Chem. Lett. 34 (2023) 108604.
[36] Y. Li, C. Zheng, S.T. Wang, et al., Angew. Chem. Int. Ed. 61 (2022) e202116563.
[37] S.T. Wang, W.H. Fang, J. Zhang, Angew. Chem. Int. Ed. 63 (2024) e20240016.
[38] S.T. Wang, Y.J. Liu, C.C. Feng, et al., Aggregate 4 (2023) e264.
[39] C.C. Feng, Z. Zhang, Z.R. Wang, et al., Inorg. Chem. 60 (2021) 1885–1892.
[40] Z.H. Liu, R.Q. Chen, S.T. Wang, et al., Eur. J. Inorg. Chem. 2022 (2022) e202200376.
[41] S. Chen, W.H. Fang, L. Zhang, Angew. Chem. Int. Ed. 57 (2018) 11252–11256.
[42] R.Y. Chen, G.H. Chen, Y.P. He, Cryst. Growth Des. 22 (2022) 66–73.
[43] L.L. Fu, Y. Fang, Z.H. Guan, et al., Nano Res. 16 (2022) 5900–5908.
[44] L.L. Fu, J. Ye, H. Li, et al., Nano Res. 15 (2022) 1355–1365.